JOURNAL OF COMPUTATIONAL PHYSICS **136,** 585–598 (1997)
ARTICLE NO. CP975783

The Computation of Spectra of Some 2D Photonic Crystals[1]

Alexander Figotin and Yuri A. Godin

Department of Mathematics, University of North Carolina at Charlotte, Charlotte, North Carolina 28223
E-mail: figotin@uncc.edu; yagodin@uncc.edu

Received October 17, 1996; revised June 2, 1997

Using analytical methods we develop an accurate and efficient algorithm for computation of the spectrum and eigenmodes for a 2D photonic crystal which comprises a periodic array of parallel rods of air of a square cross section embedded in a background lossless medium of higher dielectric constant. The numerical analysis of dependence of the spectral bands on the parameters of the 2D photonic crystal is carried out. It gives a reliable base for the optimal design of 2D photonic crystals. © 1997 Academic Press

1. INTRODUCTION

The propagation of electromagnetic (EM) waves in periodic and disordered dielectrics has attracted much attention in recent years (see [3, 25, 12–14, 21] and references therein). Periodic dielectric structures are often referred to as photonic crystals. The fundamental similarity between photonic and solid crystals lies, of course, in the media periodicity implying band structure of its spectrum and the Bloch eigenmodes [1]. In particular, if there exists a gap in the frequency spectrum of a photonic crystal, then EM waves of those frequencies will fail to propagate in the medium. The latter phenomenon is of great theoretical and practical significance and can be used for the fabrication of a variety of novel optical devices such as high efficiency lasers, laser diodes, highly efficient wave guides, optical transistors, high speed optical switches and more (see [3, 25] and references therein). The experimental results (see [24, 4, 27]) for some periodic dielectric structures suggest that photonic gap regime can be achieved and fabrication of 2D photonic crystals in the nanoscale was reported in [26].

The computation of bands and gaps and other spectral attributes for 2D photonic crystals, not to mention 3D periodic dielectrics, is a challenging numerical problem because of the high dimensions of the matrices involved. The theory of 2D photonic crystals reduces to the investigation of two scalar equations for the so-called *E*- and *H*-polarized electromagnetic fields of the Bloch form. Various theoretical methods for 2D photonic crystals were developed in [25] for sinusoidally and rectangularly modulated dielectric constants and in [16, 20] for a periodic array of parallel dielectric rods of circular cross section whose intersections with perpendicular planes form a triangular or square lattice. Similar structures were studied theoretically and experimentally in [17, 18]. All those results (see also [5, 7, 15, 22]) suggest the possibility of a gap (or pseudogap) regime for some two-component periodic dielectrics. The common approach to the computations of bands and gaps is based on the decomposition of the fields into plane waves, i.e., standard Fourier series, with the consequent series truncation. The clear advantage of this approach is that, at least theoretically, it works for any periodic dielectric structures. However, in practice, the truncation severely limits the accuracy of the plane-wave method [25, 23]. The reason for this can be briefly explained as follows. To enhance the multiple scattering which gives rise to the gaps the high contrast dielectric structures should be considered. The high contrast in the medium means strong discontinuities in the position-dependent dielectric constant $\varepsilon(x)$ and, hence, the series of plane waves for $\varepsilon(x)$ converges to it very slowly. The latter necessitates taking large numbers of plane waves, resulting in enormous dimensions of the matrices to be handled [25, 23].

Another approach to the computation of the bandgap structure is based on finite-difference approximation of Maxwell's equations. In the *T*-matrix method [19], a transfer matrix is calculated by integration of the wavefield to find the change of the electric and magnetic fields in adjacent layers of the dielectric. Unlike the *T*-matrix approach, the *R*-matrix method relates the electric field of adjacent layers to the magnetic field on both sides. A comparison of the two methods is discussed in [6].

An alternative to the plane-wave method we employ here is based on the following simple observation. The failure of the plane-wave series for a Bloch eigenmode, say Ψ, to converge well is caused by the discontinuities of Ψ and its partial derivatives associated with the discontinuity of the dielectric constant $\varepsilon(x)$. A reasonable way to

[1] The U.S. Government's right to retain a nonexclusive royalty-free license in and to the copyright covering this paper, for governmental purposes, is acknowledged.

0021-9991/97 $25.00

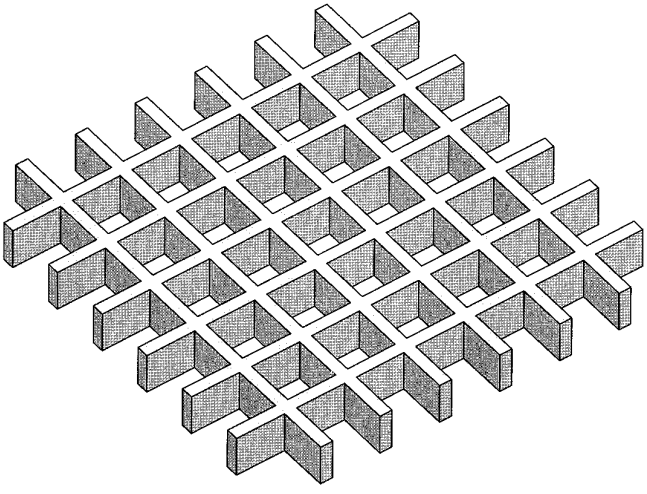

FIG. 1. A slab of 2D photonic crystal composed of lossless dielectric material embedded in air background. Only the waves propagating in the horizontal plane are considered.

overcome that kind of problem is to take, instead of plane waves, a set of orthogonal functions $\mathring{W}_{\mathbf{n}}$, called in the sequel the *basis waves*, that have appropriate discontinuities associated with $\varepsilon(x)$. Moreover, if one chooses the basis waves $\mathring{W}_{\mathbf{n}}$ which take into account more features of the medium, then the numerical implementation can be even more efficient.

The construction of the basis waves $\mathring{W}_{\mathbf{n}}$ employs eigenfunctions of auxiliary 1D Schrödinger equations that are similar to 1D equations for classical waves. For those 1D eigenproblems we develop an efficient analytical approach using a phase function allowing fast and precise computation of a large number of the 1D eigenfunctions and eigenvalues. Since such 1D eigenvalue problems arise naturally in the theory of 1D periodic Schrödinger equations with periodic potentials [1] and in problems of diffraction by lamellar dielectric grating [2], we believe that the phase method we apply here is of interest in its own right.

We consider a lossless dielectric medium shown in Fig. 1 consisting of air columns embedded in an optically dense background of dielectric constant $\varepsilon > 1$. Such a type of medium was thoroughly studied in [8–9]. Based on the analytical results for the spectrum and the Bloch eigenmodes from [8–9] we construct the basis $\{F_n\}$ as described below and then use it in the Rayleigh–Ritz procedure for numerical analysis of the spectral attributes of the medium. Computation of the spectra of some 2D photonic crystals based on [8–9] was carried out in [10] by a somewhat different approach.

Our treatment of dielectric media is based on Maxwell's equations,

$$\nabla \times \mathbf{E} = -\frac{1}{c}\frac{\partial \mathbf{B}}{\partial t}, \quad \nabla \cdot \mathbf{D} = 0, \mathbf{D} = \varepsilon \mathbf{E}, \tag{1}$$

$$\nabla \times \mathbf{H} = \frac{1}{c}\frac{\partial \mathbf{D}}{\partial t}, \qquad \nabla \cdot \mathbf{B} = 0, \mathbf{B} = \mu \mathbf{H}, \tag{2}$$

where $\mathbf{E}$, $\mathbf{D}$, $\mathbf{H}$, and $\mathbf{B}$ are the electric field and induction and the magnetic field and induction, respectively, and c is the velocity of light. We assume that $\mu \equiv 1$ (the condition that holds for many dielectric materials). The dielectric constant ε is supposed to be position-dependent and we ignore its dependence on the frequency. Denoting by x_1, x_2, x_3 and e_1, e_2, e_3 the space coordinates and the standard basis vectors we assume that $\varepsilon = \varepsilon(x_1, x_2)$ is a 2D-periodic function,

$$\varepsilon(x_1 + Ln_1, x_2 + Ln_2) = \varepsilon(x_1, x_2), \tag{3}$$

where L is the linear dimension of the square primitive cell $L[0, 1]^2$ and n_j are any integers. The space distribution of the dielectric within one cell of period, scaled by the factor L^{-1}, is shown in Fig. 2a. Note that δL is the distance between the air columns and $0 < \delta < 1$.

We will consider the waves propagating along the plane $\langle e_1, e_2 \rangle$. Then the magnetic and electric fields $\mathbf{H}$ and $\mathbf{E}$ will depend only on x_1, x_2:

$$\mathbf{H} = \mathbf{H}(x_1, x_2), \quad \nabla \cdot \mathbf{H} = 0; \quad \mathbf{E} = \mathbf{E}(x_1, x_2), \quad \nabla \cdot \varepsilon \mathbf{E} = 0. \tag{4}$$

Proceeding in the standard fashion we plug into the Maxwell equations (1)–(2) the harmonic in time fields

$$\mathbf{H}(\mathbf{x}, t) = \mathbf{H}(x_1, x_2)e^{-i\omega t}, \quad \mathbf{E}(\mathbf{x}, t) = \mathbf{E}(x_1, x_2)e^{-i\omega t}, \tag{5}$$

$$\mathbf{H} = \begin{bmatrix} H_1 \\ H_2 \\ H_3 \end{bmatrix}, \qquad \mathbf{E} = \begin{bmatrix} E_1 \\ E_2 \\ E_3 \end{bmatrix} \tag{6}$$

and arrive at the following eigenvalue problem:

$$\nabla \times \mathbf{E}(x_1, x_2) = \frac{i\omega}{c}\mathbf{H}(x_1, x_2),$$

$$\nabla \times \mathbf{H}(x_1, x_2) = -\frac{i\omega}{c}\varepsilon \mathbf{E}(x_1, x_2), \tag{7}$$

$$\nabla \cdot \varepsilon \mathbf{E}(x_1, x_2) = 0, \quad \nabla \cdot \mathbf{H}(x_1, x_2) = 0. \tag{8}$$

From now on we will denote the two component quantities (x_1, x_2), (y_1, y_2), ... by the vectors $\mathbf{x}$, $\mathbf{y}$, ..., respectively. It is convenient at this point to scale the space and other quantities of interest as

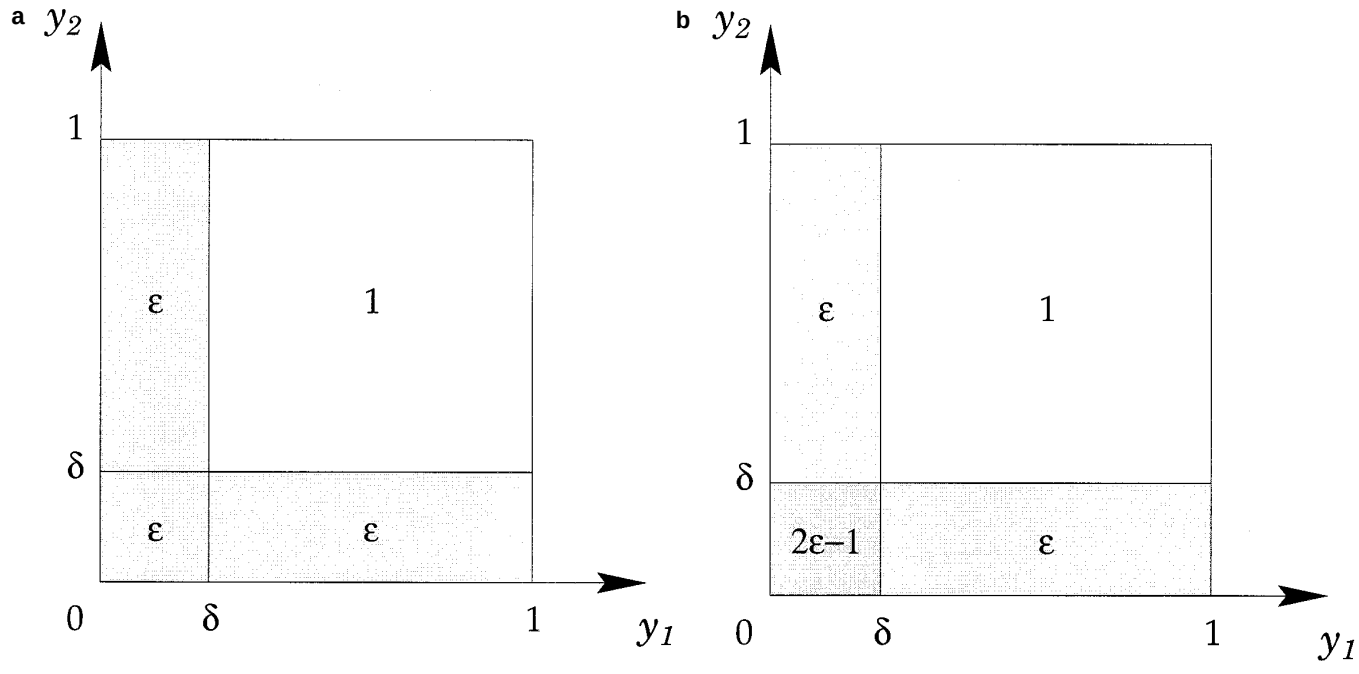

FIG. 2. Distribution of the dielectric in the cell of period (cross sections) for (a) the main problem and (b) for the auxiliary exactly solvable model.

$$y_j = x_j L^{-1}, \quad \Omega = \frac{L\omega}{c}, \quad \bar{\varepsilon}(\mathbf{y}) = \varepsilon(\mathbf{x}). \tag{9}$$

Then Eqs. (7)–(8) take the form

$$\nabla_{\mathbf{y}} \times \mathbf{E}(\mathbf{y}) = i\Omega \mathbf{H}(\mathbf{y}), \quad \nabla_{\mathbf{y}} \times \mathbf{H}(\mathbf{y}) = -i\Omega \bar{\varepsilon}(\mathbf{y})\mathbf{E}(\mathbf{y}) \tag{10}$$

$$\nabla_{\mathbf{y}} \cdot \bar{\varepsilon}(\mathbf{y})\mathbf{E}(\mathbf{y}) = 0, \quad \nabla_{\mathbf{y}} \cdot \mathbf{H}(\mathbf{y}) = 0. \tag{11}$$

The periodicity condition (3) now reads

$$\bar{\varepsilon}(\mathbf{y} + \mathbf{n}) = \bar{\varepsilon}(\mathbf{y}) \tag{12}$$

for any integer $\mathbf{n} = (n_1, n_2)$.

It is well known [11] that the spectral analysis of the problem (7)–(8) can be reduced to two scalar equations associated with two polarizations: (i) E-polarized fields (or TM modes) when $H_3 = 0$ and $E_1 = E_2 = 0$; and (ii) H-polarized fields (or TE modes) when $E_3 = 0$ and $H_1 = H_2 = 0$. Namely, for E-polarized fields the equation

$$-(\partial_1^2 + \partial_2^2)E_3(\mathbf{y}) = \Omega^2 \bar{\varepsilon}(\mathbf{y})E_3(\mathbf{y}), \partial_j = \frac{\partial}{\partial y_j} \tag{13}$$

holds, while for H polarization we have

$$-\left[\partial_1 \frac{1}{\bar{\varepsilon}(\mathbf{y})}\partial_1 + \partial_2 \frac{1}{\bar{\varepsilon}(\mathbf{y})}\partial_2\right] H_3(\mathbf{y}) = \Omega^2 H_3(\mathbf{y}). \tag{14}$$

Since $\bar{\varepsilon}(\mathbf{y})$ is a periodic function we take E_3 and H_3 in the Bloch form,

$$E_3(\mathbf{y}) = e^{i\mathbf{k}\cdot\mathbf{y}}E(\mathbf{k}, \mathbf{y}), \quad H_3(\mathbf{y}) = e^{i\mathbf{k}\cdot\mathbf{y}}H(\mathbf{k}, \mathbf{y}),$$

where $E(\mathbf{y})$ and $H(\mathbf{y})$ are periodic functions satisfying equalities similar to (12). Then plugging them into (13) and (14) we obtain

$$-(\partial_{1,k_1}^2 + \partial_{2,k_2}^2)E = \Omega^2 \bar{\varepsilon} E, \quad \partial_{j,\kappa} = \partial_j + i\kappa, 0 \le y_1, y_2 \le 1, \tag{15}$$

$$-\left[\partial_{1,k_1}\frac{1}{\bar{\varepsilon}}\partial_{1,k_1} + \partial_{2,k_2}\frac{1}{\bar{\varepsilon}}\partial_{2,k_2}\right] H = \Omega^2 H, \quad 0 \le y_1\, y_2 \le 1. \tag{16}$$

The properties of the eigenvalue problems (15) and (16) were thoroughly analyzed in [8]–[9] by analytical methods. Based on them we will proceed as follows. Let us consider first the problem (15). Following [9] we introduce the auxiliary periodic distribution of the dielectric

$$\varepsilon^\circ(\mathbf{y}) = \rho(y_1) + \rho(y_2), \rho(y) = \begin{cases} \varepsilon - \frac{1}{2}, & 0 \le y \le \delta, \\ \frac{1}{2}, & \delta < y < 1, \end{cases} \qquad \rho(y + n) = \rho(y). \tag{17}$$

and the corresponding eigenvalue problem,

$$-(\partial_{1,k_1}^2 + \partial_{2,k_2}^2)E = \Omega^2 \varepsilon^\circ(\mathbf{y})E, \quad \partial_{j,\kappa} = \partial_j + i\kappa, 0 \le y_1, y_2 \le 1. \tag{18}$$

A cross section of the medium with the dielectric constant ε° is shown in Fig. 2b. Note that the two dielectric functions $\overline{\varepsilon}(\mathbf{y})$ and $\varepsilon^\circ(\mathbf{y})$ differ only in the smaller square $[0, \delta]^2$.

Since in (18) we can separate the variables, the set of eigenvalues and eigenfunctions for the problem (18) can be parameterized by two nonnegative indices n_1 and n_2, namely, $\mathring{\Omega}_{E,n_1n_2}(k_1, k_2)$ and $\mathring{W}_{E,n_1n_2}(k_1, y_1; k_2, y_2)$, and they can be efficiently found in terms of the eigenvalues and eigenfunctions of some auxiliary eigenvalue problems (see [9] and the next sections).

Having found $\mathring{\Omega}_{E,\mathbf{n}}(\mathbf{k})$ and $\mathring{W}_{E,\mathbf{n}}(\mathbf{k}, \mathbf{y})$, we represent the eigenmode $E(\mathbf{k}, \mathbf{y})$ of Eq. (15) in terms of the waves $\mathring{W}_{E,\mathbf{n}}(\mathbf{k}, \mathbf{y})$,

$$E(\mathbf{k}, \mathbf{y}) = \sum_{n_1,n_2=0}^{N} E_{\mathbf{n}} \mathring{W}_{E,\mathbf{n}}(\mathbf{k}, \mathbf{y}) = \sum_{\mathbf{n}}^{N} E_{\mathbf{n}} \mathring{W}_{E,\mathbf{n}}(\mathbf{k}, \mathbf{y}), \quad (19)$$

where N is the truncation parameter. Then using the Rayleigh–Ritz method we seek the eigenvalues as the extreme values of the ratio of quadratic forms

$$\frac{\int_{[0,1]^2} |\nabla_{\mathbf{y}} E(\mathbf{k}, \mathbf{y})|^2 \, d\mathbf{y}}{\int_{[0,1]^2} \overline{\varepsilon}(\mathbf{y}) |E(\mathbf{k}, \mathbf{y})|^2 \, d\mathbf{y}} = \frac{\int_{[0,1]^2} |\nabla_{\mathbf{y}} \sum_{\mathbf{n}}^{N} E_{\mathbf{n}} \mathring{W}_{E,\mathbf{n}}(\mathbf{k}, \mathbf{y})|^2 \, d\mathbf{y}}{\int_{[0,1]^2} \overline{\varepsilon}(\mathbf{y}) \, |\sum_{\mathbf{n}}^{N} E_{\mathbf{n}} \mathring{W}_{E,\mathbf{n}}(\mathbf{k}, \mathbf{y})|^2 \, d\mathbf{y}} \quad (20)$$

for the vectors with coordinates $\{E_{\mathbf{n}}, 0 \le n_1, n_2 \le N\}$. The eigenfunctions will be the vectors for which the extreme values are attained.

The eigenvalues and eigenmodes for the problem (16) are found in a similar manner in terms of the eigenvalues $\mathring{\Omega}_{H,\,\mathrm{n}}(\mathbf{k})$ and eigenmodes $\mathring{W}_{H,\mathbf{n}}(\mathbf{k}, \mathbf{y})$ for the next problem,

$$-\left[\partial_{1,k_1} \frac{1}{\varepsilon_1} \partial_{1,k_1} + \partial_{2,k_2} \frac{1}{\varepsilon_2} \partial_{2,k_2}\right] H = \Omega^2 H, \quad 0 \le y_1, y_2 \le 1, \quad (21)$$

where

$$\varepsilon_j = \vartheta(y_j), \; \vartheta(y) = \begin{cases} \varepsilon, & 0 \le y < \delta, \\ 1, & \delta \le y \le 1. \end{cases} \quad (22)$$

Since the variables in (21) can be separated, we can efficiently find $\mathring{\Omega}_{H,\mathbf{n}}(\mathbf{k})$ and $\mathring{W}_{H,\mathbf{n}}(\mathbf{k}, \mathbf{y})$ in terms of some auxiliary 1D problems (see the next sections). After that we decompose $H(\mathbf{k}, \mathbf{y})$ into the waves $\mathring{W}_{H,\mathbf{n}}(\mathbf{k}, \mathbf{y})$,

$$H(\mathbf{k}, \mathbf{y}) = \sum_{n_1,n_2=0}^{N} H_{\mathbf{n}} \mathring{W}_{H,\mathbf{n}}(k, y) = \sum_{\mathbf{n}}^{N} H_{\mathbf{n}} \mathring{W}_{H,\mathbf{n}}(\mathbf{k}, \mathbf{y}), \quad (23)$$

and then we find the extreme values of the ratio of quadratic forms,

$$\frac{\int_{[0,1]^2} \overline{\varepsilon}^{-1}(\mathbf{y}) |\nabla_{\mathbf{y}} H(\mathbf{k}, \mathbf{y})|^2 \, d\mathbf{y}}{\int_{[0,1]^2} |H(\mathbf{k}, \mathbf{y})|^2 \, d\mathbf{y}} = \frac{\int_{[0,1]^2} \overline{\varepsilon}^{-1}(\mathbf{y}) \, |\nabla_{\mathbf{y}} \sum_{\mathbf{n}}^{N} H_{\mathbf{n}} \mathring{W}_{H,\mathbf{n}}(\mathbf{k}, \mathbf{y})|^2 \, d\mathbf{y}}{\int_{[0,1]^2} |\sum_{\mathbf{n}}^{N} H_{\mathbf{n}} \mathring{W}_{H,\mathbf{n}}(\mathbf{k}, \mathbf{y})|^2 \, d\mathbf{y}}, \quad (24)$$

as well as the vectors for which the extreme values are attained.

Thus, instead of *plane wave* decomposition we use decompositions (19) and (23) for the electric and magnetic fields into the waves $\mathring{W}_{E,\mathbf{n}}(\mathbf{k}, \mathbf{y})$ and $\mathring{W}_{H,\mathbf{n}}(\mathbf{k}, \mathbf{y})$, respectively, which will be referred to as *the basis waves*.

2. EIGENMODE DECOMPOSITION INTO BASIS WAVES

Here we describe how we find decomposition of the eigenmodes $W_{E,\mathbf{n}}(\mathbf{k}, \mathbf{y})$ and $W_{H,\mathbf{n}}(\mathbf{k}, \mathbf{y})$ of the main eigenvalue problems (15) and (16), respectively, on the basis waves $\mathring{W}_{E,\mathbf{n}}(\mathbf{k}, \mathbf{y})$ and $\mathring{W}_{H,\mathbf{n}}(\mathbf{k}, \mathbf{y})$. Let us start from the E-polarized waves. The waves $\mathring{W}_{E,\mathbf{n}}(\mathbf{k}, \mathbf{y})$ are the eigenmodes of the problem (18), i.e.,

$$-[\partial_1^2 + \partial_2^2] \mathring{W}_{E,\mathbf{n}}(\mathbf{k}, \mathbf{y}) = \varepsilon^\circ(\mathbf{y}) \mathring{\Omega}^2_{E,\mathbf{n}}(\mathbf{k}) \mathring{W}_{E,\mathbf{n}}(\mathbf{k}, \mathbf{y}). \quad (25)$$

This implies that the waves $\mathring{W}_{E,\mathbf{n}}(\mathbf{k}, \mathbf{y})$ are orthogonal with the weight $\varepsilon^\circ(\mathbf{y})$,

$$\int_{[0,1]^2} \varepsilon^\circ(\mathbf{y}) [\mathring{W}_{E,\mathbf{n}}(\mathbf{k}, \mathbf{y})]^* \mathring{W}_{E,\mathbf{m}}(\mathbf{k}, \mathbf{y}) \, d\mathbf{y} = 0, \quad \mathbf{n} \ne \mathbf{m}, \quad (26)$$

where * stands for complex conjugation. After normalization

$$\int_{[0,1]^2} \varepsilon^\circ(\mathbf{y}) |\mathring{W}_{E,\mathbf{n}}(\mathbf{k}, \mathbf{y})|^2 \, d\mathbf{y} = 1, \quad (27)$$

condition (26) becomes

$$\int_{[0,1]^2} \varepsilon^\circ(\mathbf{y}) [\mathring{W}_{E,\mathbf{n}}(\mathbf{k}, \mathbf{y})]^* \mathring{W}_{E,\mathbf{m}}(\mathbf{k}, \mathbf{y}) \, d\mathbf{y} = \delta_{\mathbf{nm}}. \quad (28)$$

In addition to that, in view of (25) and (28) we get

$$\int_{[0,1]^2} [\nabla_{\mathbf{y}} \mathring{W}_{E,\mathbf{n}}(\mathbf{k}, \mathbf{y})]^* \nabla_{\mathbf{y}} \mathring{W}_{E,\mathbf{m}}(\mathbf{k}, \mathbf{y})\, d\mathbf{y} = \mathring{\Omega}^2_{E,\mathbf{n}}(\mathbf{k}) \delta_{\mathbf{nm}}. \quad (29)$$

Hence, the ratio (20) takes the form

$$\frac{\sum_{\mathbf{n}}^N \mathring{\Omega}^2_{E,\mathbf{n}}(\mathbf{k}) |E_{\mathbf{n}}|^2}{\sum_{\mathbf{n}}^N |E_{\mathbf{n}}|^2 - \sum_{\mathbf{n},\mathbf{m}}^N B_{\mathbf{nm}} E^*_{\mathbf{n}} E_{\mathbf{m}}}, \quad (30)$$

where

$$B_{\mathbf{nm}} = \int_{[0,1]^2} [\varepsilon^\circ(\mathbf{y}) - \overline{\varepsilon}(\mathbf{y})][\mathring{W}_{E,\mathbf{n}}(\mathbf{k}, \mathbf{y})]^* \mathring{W}_{E,\mathbf{m}}(\mathbf{k}, \mathbf{y})\, d\mathbf{y} \quad (31)$$

and we arrive at the eigenvalue problem

$$A_E \Psi = \Omega^2 (I - B)\Psi, \quad A_{E,\mathbf{nm}} = \mathring{\Omega}^2_{E,\mathbf{n}}(\mathbf{k}) \delta_{\mathbf{nm}}. \quad (32)$$

Solving the eigenvalue problem (32) we find the eigenvalues $\Omega_{E,\mathbf{n}}(\mathbf{k})$ which approximate the eigenvalues of the main problem (15) and the corresponding eigenvectors $\{E_{\mathbf{n};\mathbf{m}}(\mathbf{k})$, $0 \le m_1, m_2 \le N\}$, $0 \le n_1, n_2 \le N$. They both depend, in particular, on the truncation parameter N. The eigenmodes $W_{E,\mathbf{n}}(\mathbf{k}, \mathbf{y})$ of the problem (15) by virtue of (19) are represented now as

$$W_{E,\mathbf{n}}(\mathbf{k}, \mathbf{y}) = \sum_{m_1,m_2=0}^{N} E_{\mathbf{n};\mathbf{m}}(\mathbf{k}) \mathring{W}_{E,\mathbf{m}}(\mathbf{k}, \mathbf{y}). \quad (33)$$

In the case of H-polarized waves, we recall that the waves $\mathring{W}_{H,\mathbf{n}}(\mathbf{k}, \mathbf{y})$ are the eigenmodes of the problem (21) and it is easy to see that the ratio (24) takes the form

$$\frac{\sum_{\mathbf{n}}^N A_{H;\mathbf{nm}}(\mathbf{k}) |H_{\mathbf{n}}|^2}{\sum_{\mathbf{n}}^N |H_{\mathbf{n}}|^2}, \quad (34)$$

where the elements $A_{H;\mathbf{n},\mathbf{m}}$ of the matrix $A_H(\mathbf{k})$ are defined by

$$A_{H;\mathbf{nm}}(\mathbf{k}) = \int_{[0,1]^2} \overline{\varepsilon}^{-1}(\mathbf{y}) [\nabla_{\mathbf{y}} \mathring{W}_{E,\mathbf{n}}(\mathbf{k}, \mathbf{y})]^* \nabla_{\mathbf{y}} \mathring{W}_{E,\mathbf{m}}(\mathbf{k}, \mathbf{y})\, d\mathbf{y}. \quad (35)$$

Consequently, we obtain the eigenvalue problem

$$A_H \Psi = \Omega^2 \Psi, \quad (36)$$

Similar to (32), the eigenvalues $\Omega_{H,\mathbf{n}}(\mathbf{k})$, approximating the eigenvalues of the main problem (16), and the corresponding eigenvectors $\{H_{\mathbf{n};\mathbf{m}}(\mathbf{k})$, $0 \le m_1, m_2 \le N\}$, $0 \le n_1, n_2 \le N$, are found from (36) by truncation. Then the eigenmodes $W_{H,\mathbf{n}}(\mathbf{k}, \mathbf{y})$ of (16) can be found from (23) as

$$W_{H,\mathbf{n}}(\mathbf{k}, \mathbf{y}) = \sum_{m_1,m_2=0}^{N} H_{\mathbf{n};\mathbf{m}}(\mathbf{k}) \mathring{W}_{H,\mathbf{m}}(\mathbf{k}, \mathbf{y}). \quad (37)$$

3. CONSTRUCTION OF THE BASIS WAVES

Let us describe the basis waves $\mathring{W}_{E,\mathbf{n}}(\mathbf{k}, \mathbf{y})$ and $\mathring{W}_{H,\mathbf{n}}(\mathbf{k}, \mathbf{y})$ using the analytical methods developed in [8–9].

For E-polarized waves we introduce the 2D Schrödinger operator with a periodic potential,

$$S_g \psi(y_1, y_2) = [-(\partial_1^2 + \partial_2^2) - g(\rho(y_1) + \rho(y_2) - 1)]\psi(y_1, y_2), \quad (38)$$

with a parameter g and 1D Schrödinger operator,

$$s_{D,\kappa}\psi(y) = -\psi''(y) - q_{D,\delta}(y)\psi(y), \quad 0 \le y \le 1, \quad (39)$$

$$\psi(1) = e^{i\kappa}\psi(0), \quad \psi'(1) = e^{i\kappa}\psi'(0), \quad (40)$$

where

$$q_{D,\delta}(y) = \begin{cases} D\delta^{-1}, & 0 \le y < \delta \\ 0, & \delta \le y \le 1. \end{cases} \quad (41)$$

If $\xi_n(\kappa, D)$ and $f_n(\kappa, D; y)$, $n = 0, 1, \ldots$, are respectively the eigenvalues and the eigenfunctions of $s_{D,\kappa}$ then the eigenvalues $\xi_{\mathbf{n}}(\mathbf{k}, g)$ and the eigenfunctions $F_{\mathbf{n}}(\mathbf{k}, g, y_1, y_2)$ of S_g can be easily found through its one-dimensional counterparts as

$$\xi_{\mathbf{n}}(\mathbf{k}, g) = \xi_{n_1}(k_1, g\delta(\varepsilon - 1)) + \xi_{n_2}(k_2, g\delta(\varepsilon - 1)), \quad (42)$$

$$F_{\mathbf{n}}(\mathbf{k}, g; \mathbf{y}) = e^{-i(k_1 y_1 + k_2 y_2)} f_{n_1}(k_1, g\delta(\varepsilon - 1); y_1)\, f_{n_2}(k_2, g\delta(\varepsilon - 1); y_2). \quad (43)$$

Now the eigenvalues $\mathring{\Omega}_{E,\mathbf{n}}(\mathbf{k})$ are obtained as solutions Ω of the transcendental equation

$$\xi_{\mathbf{n}}(\mathbf{k}, \Omega^2) = \Omega^2 \quad (44)$$

and the corresponding eigenfunctions $\mathring{W}_{E,\mathbf{n}}(\mathbf{k}, \mathbf{y})$ then become

$$\mathring{W}_{E,\mathbf{n}}(\mathbf{k}, \mathbf{y}) = F_{\mathbf{n}}(\mathbf{k}, \mathring{\Omega}^2_{E,\mathbf{n}}(\mathbf{k}); \mathbf{y}). \quad (45)$$

For H polarization we introduce the auxiliary 1D operator

$$p_\kappa \psi(y) = -(\vartheta^{-1}(y)\psi')'(y), \quad 0 \le y \le 1, \quad (46)$$

$$\psi(1) = e^{i\kappa}\psi(0), \quad \psi'(1) = e^{i\kappa}\psi'(0), \quad (47)$$

where θ is defined by (22). If $\zeta_n(\kappa)$ and $h_n(\kappa; y)$, $n = 0, 1, ...$, are respectively the eigenvalues and the eigenfunctions of p_κ then the eigenvalues $\mathring{\Omega}^2_{H,\mathbf{n}}(\mathbf{k})$ and the eigenfunctions $\mathring{W}_{H,\mathbf{n}}(\mathbf{k}, \mathbf{y})$ of S_g can be represented as

$$\mathring{\Omega}^2_{H,\mathbf{n}}(\mathbf{k}) = \zeta_{n_1}(k_1) + \zeta_{n_2}(k_2), \tag{48}$$

$$\mathring{W}_{H,\mathbf{n}}(\mathbf{k}, \mathbf{y}) = e^{-i(k_1 y_1 + k_2 y_2)} h_{n_1}(k_1; y_1) h_{n_2}(k_2; y_2). \tag{49}$$

We remind that $\mathring{W}_{E,\mathbf{n}}(\mathbf{k}, \mathbf{y})$ and $\mathring{W}_{H,\mathbf{n}}(\mathbf{k}, \mathbf{y})$ are periodic functions of $\mathbf{y}$, i.e.,

$$\mathring{W}_{E,\mathbf{n}}(\mathbf{k}, \mathbf{y} + \mathbf{m}) = \mathring{W}_{E,\mathbf{n}}(\mathbf{k}, \mathbf{y}) \tag{50}$$

$$\mathring{W}_{H,\mathbf{n}}(\mathbf{k}, \mathbf{y} + \mathbf{m}) = \mathring{W}_{H,\mathbf{n}}(\mathbf{k}, \mathbf{y}) \tag{51}$$

for all $\mathbf{m}$ with integer-valued components.

4. AUXILIARY 1D PROBLEMS: THE PHASE METHOD

In this section we develop a phase method for the efficient computation of the eigenvalues of the auxiliary 1D operators (39)–(40) and (46)–(47). These eigenvalue problems are similar to those arising in 1D periodic solids [1], wave propagation in two component layered media, and diffraction by lamellar dielectric grating (see [2] and references therein).

4.1. *E–Polarized Wave*

Consider the Schrödinger operator $s_{D,\kappa}$ defined by (39)–(40) and the corresponding eigenvalue problem

$$s_{D,\kappa}\psi(y) = \xi\psi(y), \quad 0 \le y \le 1. \tag{52}$$

The eigenvalues $\xi_n(\kappa, D)$ of the problem (52) can be found as the solutions for ξ of the discriminant equation

$$\begin{aligned} &\cos T \cos(\sqrt{\xi}(1-\delta)) \\ &\quad - \left(\frac{D}{2} + \xi\delta\right) \frac{\sin T}{T} \frac{\sin(\sqrt{\xi}(1-\delta))}{\fallingdotseq \sqrt{\xi}} = \cos\kappa, \\ &\quad T = \delta\sqrt{D\delta^{-1} + \xi}. \end{aligned} \tag{53}$$

Then the eigenfunctions $f_n(\kappa, D; y)$ of (52) are represented as

$$f(\kappa, D; \xi_n; y) = \begin{cases} \alpha_{11}\cos(P_1 y) + \alpha_{12}\sin(P_1 y), & 0 \le y < \delta, \\ \alpha_{21}\cos(P_2(y-\delta)) + \alpha_{22}\sin(P_2(y-\delta)), & \delta \le y < 1, \end{cases} \tag{54}$$

with

$$\alpha_{11} = P_2^{-1}\cos(P_1\delta)\sin(P_2(1-\delta)) + P_1^{-1}\cos(P_2(1-\delta))\sin(P_1\delta), \tag{55}$$

$$\alpha_{12} = (P_1P_2)^{-1}[0.5D\delta^{-1}\sin(P_1\delta)\sin(P_2(1-\delta)) + iP_1P_2\sin\kappa], \tag{56}$$

$$\alpha_{21} = P_2^{-1}\sin(P_2(1-\delta)) + P_1^{-1}\sin(P_1\delta)e^{i\kappa}, \tag{57}$$

$$\alpha_{22} = P_2^{-1}[e^{i\kappa}\cos(P_1\delta) - \cos(P_2(1-\delta))], \tag{58}$$

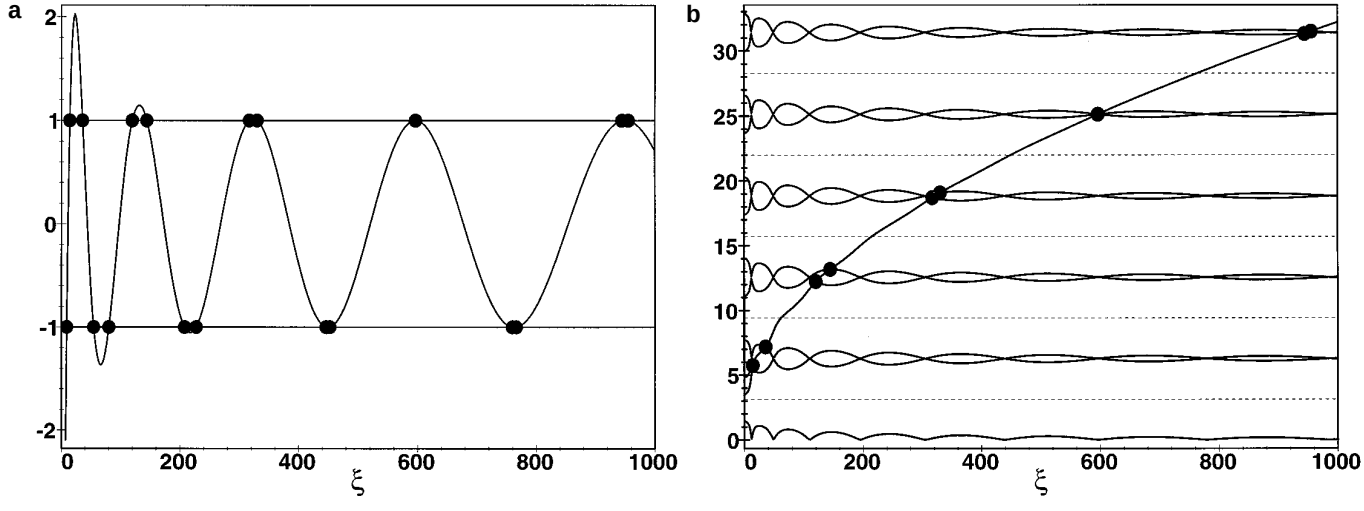

FIG. 3. A typical graph (a) of the discriminant equation (53). Intersection points of the curve with the straight lines ± 1 (corresponding to $\kappa = 0, \pi$) are solutions of Eq. (53). Their separation becomes a challenging problem for large ξ. After representation (64)–(65) the phase curve Ψ_E has only one intersection with the horizontal curves in the given interval. Bold points in (b) correspond to intersections of the discriminant curve with the line $+1$.

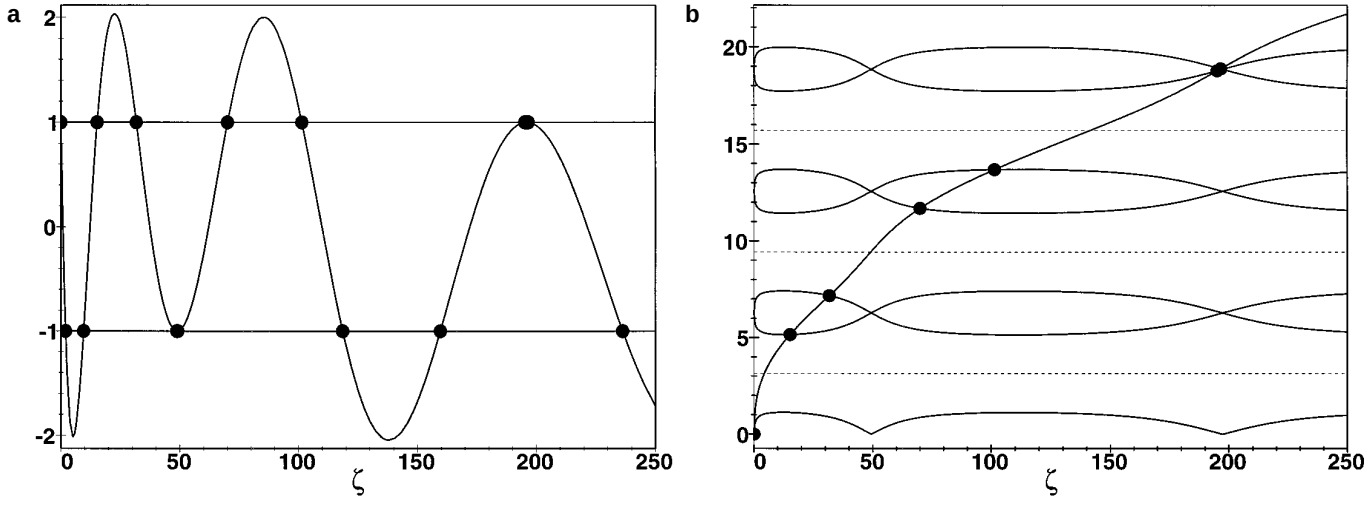

FIG. 4. A typical graph (a) of the discriminant equation (67). Intersection points of the curve with the lines ± 1 (corresponding to $\kappa = 0, \pi$) are solutions of Eq. (67). Their computation becomes a challenging problem for closely-spaced ζ_n. After representation (77)–(78) the phase curve Ψ_H has only one intersection with the horizontal curves in the given interval. Bold points in (b) correspond to intersections of the discriminant curve with the line $+1$.

$$P_1 = \sqrt{D\delta^{-1} + \xi_n}, \quad P_2 = \sqrt{\xi_n}. \tag{59}$$

From a typical graph of (53) for $\kappa = 0, \pi$ shown in Fig. 3a one can see that numerical separation of neighboring ξ_n becomes a challenging problem as ξ increases. To remedy this, let us rewrite (53) in the phase form

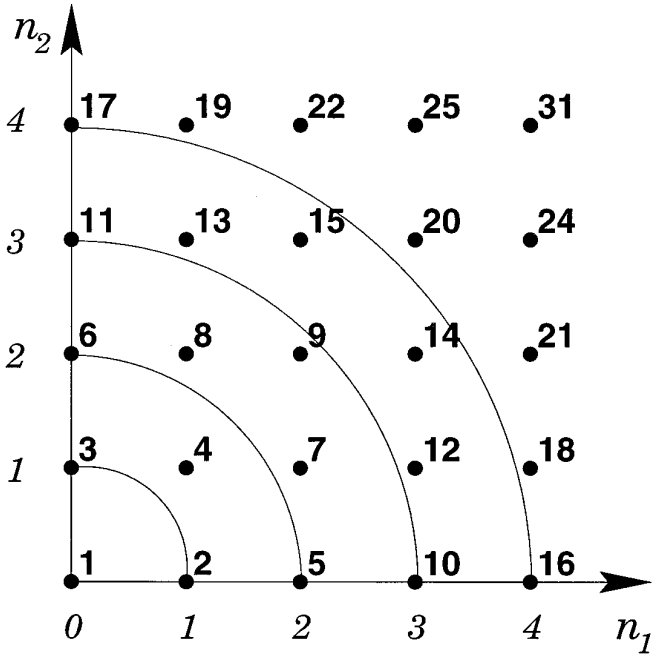

FIG. 5. Pattern for enumeration of two-dimensional integer points $\mathbf{n} = (n_1, n_2)$ by integer numbers according to their proximity to the origin.

$$A_E(D, \delta, T)\cos\Psi_E(D, \delta, T) = \cos\kappa, \tag{60}$$

where

$$A_E(D, \delta, T) = \begin{cases} \sqrt{1 + \nu\sinh^2\alpha}, & 0 \le T \le \sqrt{d}, \\ \sqrt{1 - \nu\sin^2\alpha}, & T \ge \sqrt{d}, \end{cases} \tag{61}$$

$$\Psi_E(D, \delta, T) = \begin{cases} T + \arctan(\nu_1 \tanh\alpha), & 0 \le T \le \sqrt{d}, \\ T + \alpha + \arctan\left(q\dfrac{\sin 2\alpha}{1 - q\cos 2\alpha}\right), & T \ge \sqrt{d}, \end{cases} \tag{62}$$

$$d = D\delta, \alpha = \frac{(1-\delta)\sqrt{|d - T^2|}}{\delta}, \tag{63}$$

$$\nu = \frac{d^2}{4T^2(d - T^2)}, \quad \nu_1 = \frac{1}{2}\frac{2T^2 - d}{T\sqrt{|T^2 - d|}}, \quad q = \frac{\nu_1 - 1}{\nu_1 + 1}.$$

Observe that the phase $\Psi_E(D,\delta, T)$ is an increasing function of T and the amplitude $A_E(D, \delta, T) \ge 1$. Now the solution of (60) is reduced to the transcendental equation for T,

$$\Psi_E(D, \delta, T) = = \begin{cases} 2\pi n + \eta \\ 2\pi n - \eta \end{cases}, \quad n = 0, 1, ..., \tag{64}$$

$$\eta = \arccos\left(\frac{\cos\kappa}{A_E(D, \delta; T)}\right), \quad 0 \le \eta \le \pi. \tag{65}$$

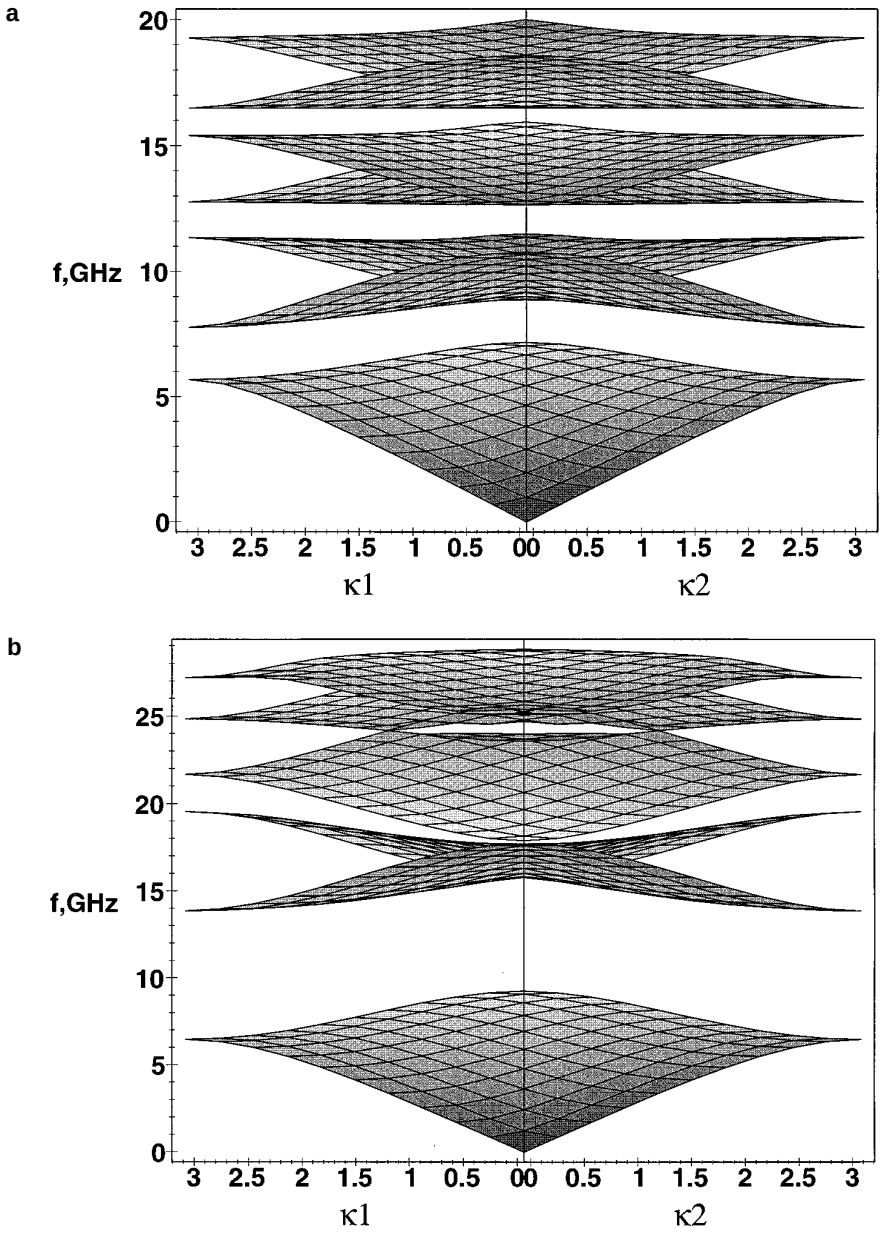

FIG. 6. Profile of the spectral surfaces (dispersion relations) $f_n(\kappa_1, \kappa_2) = \omega_n(\kappa_1, \kappa_2)/2\pi$ for (a) E and (b) H polarization. The plane $\langle \kappa_1, \kappa_2 \rangle$ is perpendicular to paper. The views show gaps in both spectra. Due to the symmetry one quarter of each Brillouin zone is shown. $\varepsilon = 20$, $\delta = 0.1$, $L = 1$ cm.

Since the phase $\Psi_E(D, \delta; T)$ is an increasing function of T and $A_E(D, \delta; T) \geq 1$ then for any integer n and nonnegative D Eqs. (64)–(65) clearly have a unique solution for T. Its graphical representation is given in Fig. 3b. Note that near the point $\xi = 596$ in Figs. 3a and 3b there are two closely spaced eigenvalues (which can even merge into one of multiplicity two for some values of ε and δ) lying on the straight line $+1$. However, in Fig. 3b, after the phase transformation, there is always exactly one intersection point of the phase curve with each of the horizontal lines.

4.2. *H–Polarized Waves*

Consider the operator p_κ defined by (46)–(49) and the corresponding eigenvalue problem

$$p_\kappa h(y) = \zeta h(y), \quad 0 \leq y \leq 1. \tag{66}$$

The eigenvalues $\zeta_n(\kappa)$ of the problem (66) can be found from the discriminant equation

TABLE I

Spectrum Bands of E and H-Polarized Waves for $\varepsilon = 20$, $\delta = 0.1$, $L = 1$ cm

Zone	E-band, GHz	H-band, GHz
1	[0.00, 7.10]	[0.00, 9.21]
2	[7.76, 10.8]	[13.9, 17.7]
3	[8.85, 11.3]	[15.8, 19.5]
4	[12.7, 14.9]	[17.8, 24.0]
5	[12.7, 15.7]	[24.1, 28.1]
6	[16.4, 18.6]	[25.3, 28.7]

Note. Numbering of zones does not take into account their multiplicity. An absolute band gap occurs in the interval [11.3 − 12.7] GHz.

$$\cos(\sqrt{\zeta}(1-\delta))\cos(\sqrt{\zeta\varepsilon}\delta) - \frac{\varepsilon^{1/2}+\varepsilon^{-1/2}}{2}\sin(\sqrt{\zeta}(1-\delta))\sin(\sqrt{\varepsilon}\delta) = \cos\kappa. \tag{67}$$

The eigenfunctions $h_n(\kappa; y)$ then have the representation

$$h(\kappa;\zeta_n;y) = \begin{cases} \beta_{11}\cos\sqrt{\zeta_c\varepsilon}y + \beta_{12}\sin(\sqrt{\zeta_n\varepsilon}y), & 0 \le y < \delta, \\ \beta_{21}\cos(\sqrt{\zeta_n}(y-\delta)) + \beta_{22}\sin(\sqrt{\zeta_n}(y-\delta)), & \delta \le y < 1, \end{cases} \tag{68}$$

where

$$\beta_{11} = -\frac{\sin\nu\cos\tau + \sqrt{\varepsilon}\cos\nu\sin\tau}{\sqrt{\zeta}\,\varepsilon}, \tag{69}$$

$$\beta_{12} = \frac{\sqrt{\varepsilon}\cos\nu\cos\tau - \sqrt{\varepsilon}e^{i\kappa} - \sin\nu\sin\tau}{\sqrt{\zeta_n}\,\varepsilon}, \tag{70}$$

$$\beta_{21} = \frac{\sin\nu - \sqrt{\varepsilon}e^{i\kappa}\sin\tau}{\sqrt{\zeta_n}\varepsilon}, \quad \beta_{22} = -\frac{\cos\nu - e^{i\kappa}\cos\tau}{\sqrt{\zeta_n}\varepsilon}, \tag{71}$$

$$\nu = \sqrt{\zeta_n}(1-\delta), \quad \tau = \sqrt{\zeta_n\varepsilon}\delta. \tag{72}$$

Similar to Eq. (53), solutions ζ_n of (67) may be closely spaced (Fig. 4a) that makes the computation difficult. The form of (67) which is convenient for computation of eigenvalues may be taken as

$$A_H(\delta,\varepsilon;\zeta)\cos\Psi_H(\delta,\varepsilon;\zeta) = \cos\kappa, \tag{73}$$

where

$$A_H(\delta,\varepsilon,\zeta) = \sqrt{1+(f-1)\sin^2\tau}, \quad \tau = \sqrt{\zeta\varepsilon}\delta, \tag{74}$$

$$\Psi(\delta,\varepsilon;\zeta) = \nu + \tau + \arctan\left(q\frac{\sin 2\tau}{1-q\cos 2\tau}\right),$$

$$\nu = \sqrt{\zeta}(1-\delta), \tag{75}$$

$$f = \frac{\varepsilon+\varepsilon^{-1}+2}{4}, \quad q = \frac{f_1-1}{f_1+1},$$

$$f_1 = \frac{\varepsilon^{1/2}+\varepsilon^{-1/2}}{2}. \tag{76}$$

Note that as in the case of E polarization the phase $\Psi_H(\delta,\varepsilon;\zeta)$ is an increasing function of ζ and the amplitude $A_H(\delta,\varepsilon;\zeta) \ge 1$. Now the eigenvalues $\zeta_n(\kappa)$ of problem (67) can be found as the solutions of the problem

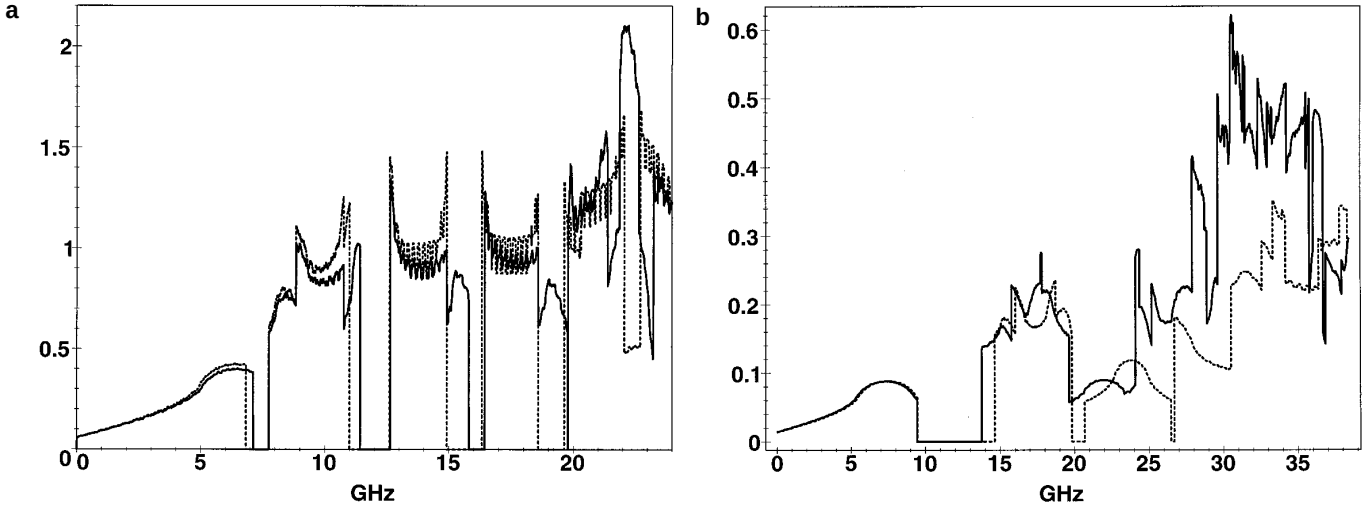

FIG. 7. Density of states for (a) E-polarization and (b) H-polarization for $\varepsilon = 20$, $\delta = 0.1$, $L = 1$ cm. The solid lines correspond to the main problems (15)–(16) with the distribution of the dielectric shown in Fig. 2a. The dashed curves refer to the auxiliary separable model whose distribution of the dielectric is shown in Fig. 2b for E-polarization (a) and is given by (22) in the case (b) of H-polarization.

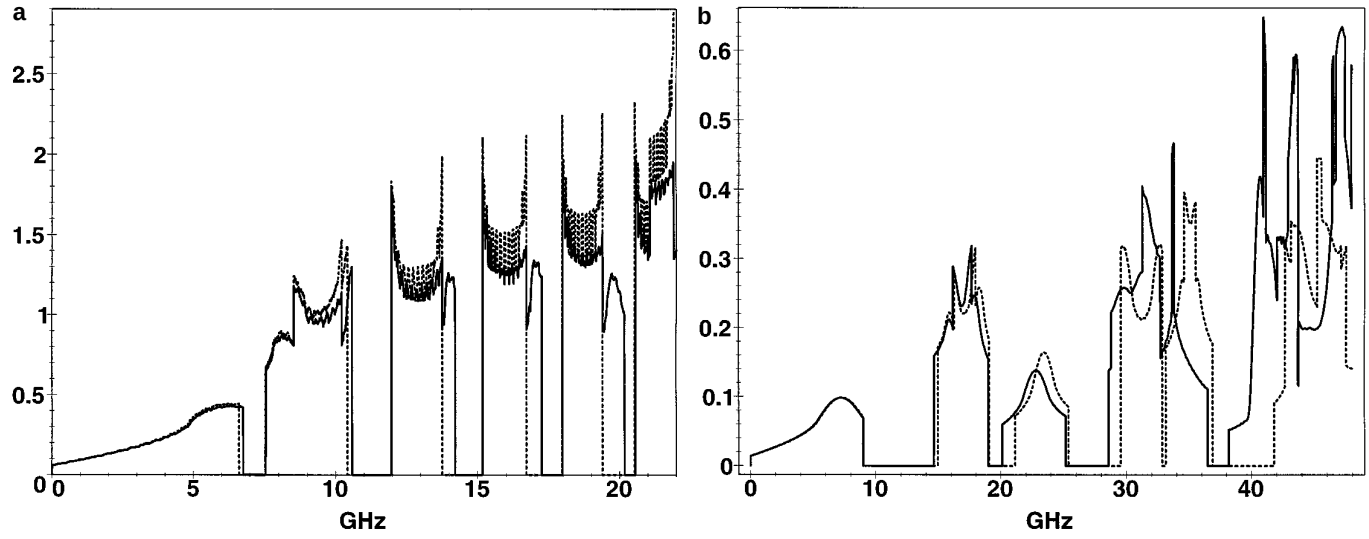

FIG. 8. Density of states for (a) E-polarization and (b) H-polarization for $\varepsilon = 50$, $\delta = 0.04$, $L = 1$ cm. The solid lines correspond to the main problems (15)–(16) with the distribution of the dielectric shown in Fig. 2a. The dashed curves refer to the auxiliary separable model whose distribution of the dielectric is shown in Fig. 2b for E-polarization (a) and is given by (22) in the case (b) of H-polarization.

$$\Psi_H(\delta, \varepsilon; \zeta) = \begin{cases} 2\pi n + \eta \\ 2\pi n - \eta \end{cases}, \quad n = 0, 1, ..., \tag{77}$$

$$\eta = \arccos\left(\frac{\cos\kappa}{A_H(\delta, \varepsilon; \zeta)}\right), \quad 0 \le \eta \le \pi. \tag{78}$$

Since the phase $\Psi_H(\delta, \varepsilon; \zeta)$ is an increasing function of ζ and $A_H(\delta, \varepsilon; \zeta) \ge 1$ the problem (77)–(78) clearly has a unique solution. Its graphical representation is given in Fig. 4b. In this case, as in Fig. 3a, after the phase representation two closely spaced points near $\zeta = 196$ in Fig. 4a now lie on different curves in Fig. 4b.

5. SPECTRAL ATTRIBUTES COMPUTATION

In this section we compute the spectra, dispersion relations, and eigenmodes for some values of ε and δ. The computation of the eigenvalues $\Omega_{E,\mathbf{n}}(\mathbf{k})$, $\Omega_{H,\mathbf{n}}(\mathbf{k})$, $\Omega_{E,\mathbf{n}}(\mathbf{k})$, and $\mathring{\Omega}_{H,\mathbf{n}}(\mathbf{k})$ and the eigenfunctions $W_{E,\mathbf{n}}(\mathbf{k}, \mathbf{y})$, $W_{H,\mathbf{n}}(\mathbf{k}, \mathbf{y})$, $\mathring{W}_{E,\mathbf{n}}(\mathbf{k}, \mathbf{y})$ and $\mathring{W}_{H,\mathbf{n}}(\mathbf{k},\mathbf{y})$ is based on the formulas described in the previous sections. We recall that the actual spectral band for an index $\mathbf{n}$ and, say E polarization, is an interval run by the quantity $\Omega_{E,\mathbf{n}}(\mathbf{k})$ as k_1 and k_2 run over the interval $[-\pi, \pi]$.

For numerical solution of the eigenvalue problems we need to enumerate the eigenvalues and eigenfunctions involved by one-dimensional indices. To this end, let us enumerate two-dimensional integer points by integer numbers according to their proximity to the origin and in the counterclockwise direction. The correspondence between positive integer index ν and indices $\mathbf{n}$ is shown in Fig. 5.

5.1. *Band and Gap Computation*

Calculations confirm the initial assumption of the faster convergence of the method over Fourier transform approach (the plane-wave method). To obtain the first four photonic bands of E- and H-polarized waves within 1% accuracy it is required $N = 26$ basis functions in the Rayleigh–Ritz method. As in the 1D case, band boundaries correspond to $\kappa_{1,2} = 0$ or $\kappa_{1,2} = \pi$. For every wave vector $\kappa = (\kappa_1, \kappa_2)$ we calculate N eigenvalues of Eqs. (15) and (16). When κ runs over the square $(0, \pi) \times (0, \pi)$ (one quarter of the Brillouin zone) the eigenvalues of the problems (15) and (16) sweep the dispersion surfaces. Figure 6 shows profiles of several first dispersion surfaces for E- and H-polarized waves for $\varepsilon = 20$ and $\delta = 0.1$. The clearance between the surfaces indicates the existence of gaps. All results of the computation given below are obtained for the cell length of 1 cm.

For those data there exist three gaps for E-polarization, and one gap for H-polarization above which all dispersion surfaces are overlapped.

Both E and H spectra reveal the existence of an absolute band gap in the interval [11.3–12.7] GHz shown in Table I.

Figure 7a shows the density of states for E-polarization when $\varepsilon = 20$ and $\delta = 0.1$, computed with 1681 uniformly spaced values of (κ_1, κ_2) inside one-quarter of the Brillouin zone. The solid line corresponds to the main problem (15) with the distribution of the dielectric shown in Fig. 2a. The dashed curve refers to the auxiliary separable model (18) with the dielectric distribution presented in Fig. 2b. In Fig. 7b we present the density of states for H polarization for $\varepsilon = 20$ and $\delta = 0.1$. The solid line represents the main

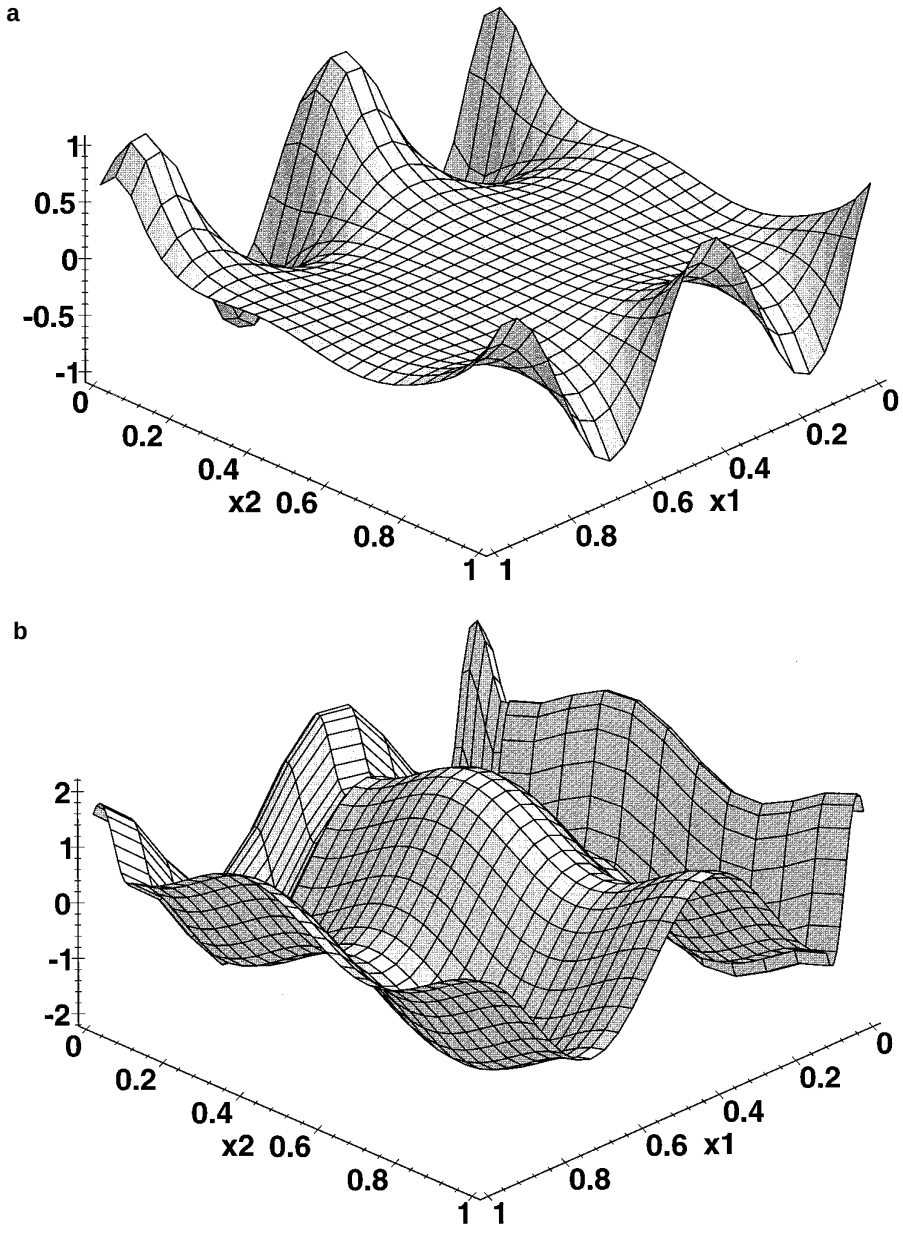

FIG. 9. Typical distributions of E (a) and H polarized (b) Bloch eigenfunctions for one cell of period: $\varepsilon = 20$, $\delta = 0.1$, $L = 1$ cm.

problem (16) corresponding to the distribution of the dielectric in Fig. 2a while the dashed line is obtained for the auxiliary separable model (21) having the dielectric distribution (22). Although conditions

$$\varepsilon\delta \gg 1 \quad \text{and} \quad \varepsilon\delta^{3/2} \ll 1 \tag{79}$$

which guarantee (see [8–9]) proximity of the results of the main and auxiliary problems do not hold, the first bands of the two problems correspond closely. The better condition (79) holds the more pronounced the agreement between the two problems is. Figure 8 shows the distribution of the density of states for $\varepsilon = 50$ and $\delta = 0.04$. For these data conditions (79) is more pronounced and, as a result, the first two bands for E- and H-polarized waves are in good agreement with the auxiliary model.

5.2. *Eigenmode Computation*

The computation of eigenmodes for E-polarization is based on the Rayleigh–Ritz method (relations (32), (33)); for H-polarization it is based on (36) and (37). Typical distributions of E- and H-polarized normalized eigenfunc-

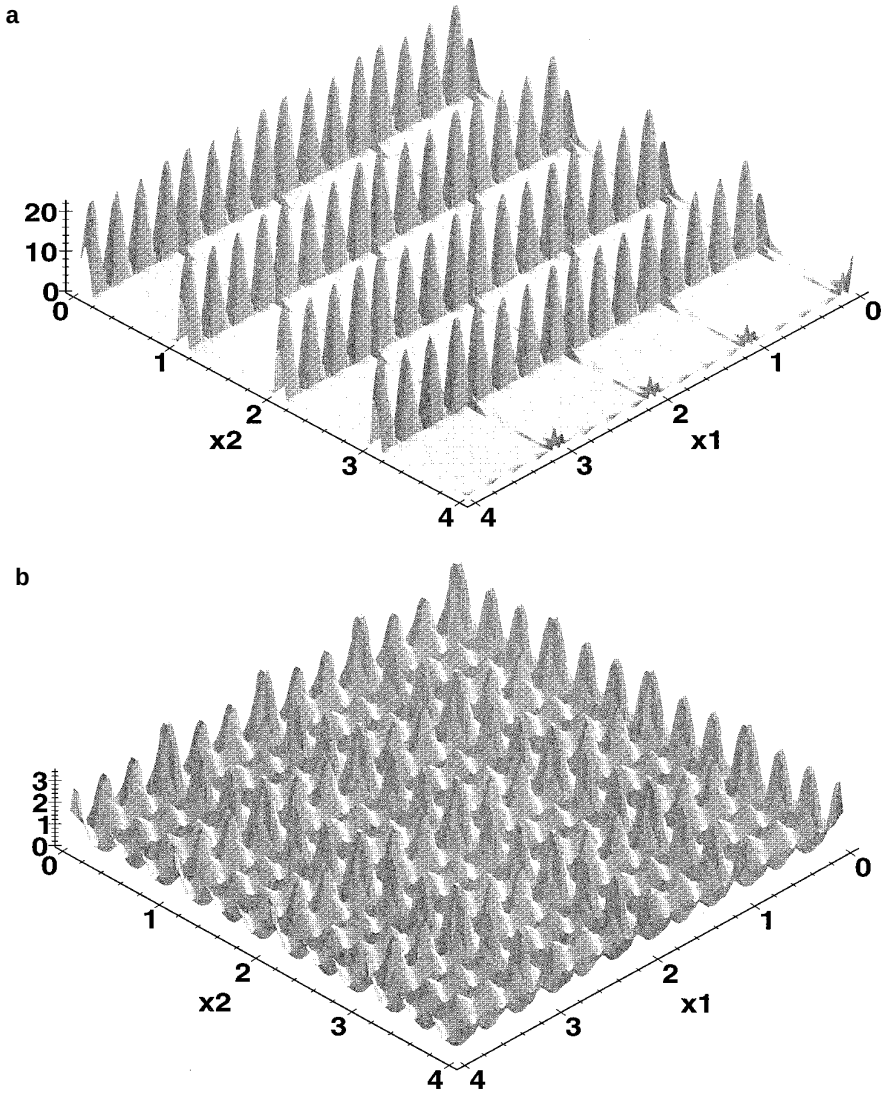

FIG. 10. Typical distributions of the energy associated with E (a) and H polarized (b) Bloch eigenfunctions for the eigenmodes shown in Fig. 9 in a specimen containing 4×4 primitive cells: $\varepsilon = 20$, $\delta = 0.1$, $L = 1$ cm.

tions for the frequencies 27.6 GHz and 49.2 GHz, respectively, are presented in Fig. 9. It shows that the electric field propagates mainly in the dielectric while the major part of the energy of H-polarized waves is concentrated in the air columns. This statement is clearly illustrated in Fig. 10 by the energy distribution of the eigenmodes plotted in Fig. 9, in a specimen containing 4×4 primitive cells. The energy of E-polarized waves is almost entirely concentrated in the dielectric walls, whereas the energy of H-polarized waves is distributed uniformly, in the average, over the primitive cell.

6. SPECTRUM DEPENDENCE ON THE MEDIUM

Fast performance of the program makes it possible to plot the band-gap diagram for a wide range of ε, thus investigating the spectrum distribution on the dielectric parameter of the lattice for a given geometry. Figure 11 shows the dependence of photonic bands and gaps for E- (a) and H-polarized (b) waves for $\delta = 0.1$. The second gap is the widest out of three gaps of E-polarized waves, whereas H-polarized waves have only one wide gap in the given range of ε.

7. ACCURACY ANALYSIS

Results of the computations were checked in different ways. The spectra of E- and H-polarized waves completely agree with those in the asymptotic case (79) for which exact estimates were obtained in [8–9]. Truncation analysis shows that for $\varepsilon = 20$ and $\delta = 0.1$ it requires 146 basis functions in the Rayleigh–Ritz method to get the 10 first

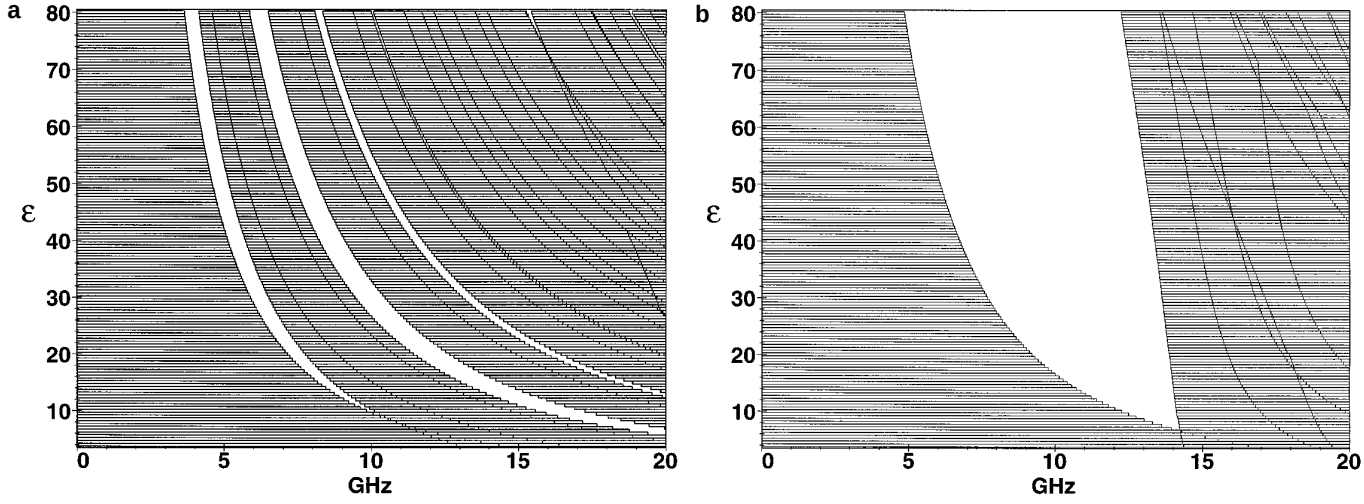

FIG. 11. Dependence of photonic bands and gaps on the dielectric constant ε for E (a) and H polarized (b) waves for $\delta = 0.1$ and $L = 1$ cm. The hatched regions correspond to the spectral bands. Unshaded regions represent spectral gaps.

spectral bands of E- and H-polarized waves with an accuracy of four significant digits.

A peculiarity of the roots of the discriminant equations (53) and (67) which was revealed in its solution should also be mentioned. It turned out that for some pairs of ε and δ the graph of the discriminant equations can be tangent to the lines $\cos \kappa = \pm 1$; i.e., the roots at those points are of multiplicity two and the basis functions become linearly dependent (Figs. 3a and 4a). To circumvent this problem and not complicate the program, we calculated the roots for κ in very close proximity to 0 and π. In this case the accuracy of computation has not been affected within four digits, since the dispersion surfaces have horizontal tangent planes at those points.

8. CONCLUSIONS

Based on analytical methods from [8, 9] we developed the algorithms for precise computation of bands and gaps of the frequency spectrum, the dispersion relations, and the Bloch eigenmodes for 2D photonic crystals consisting of a periodic array of air columns of a square cross section embedded in an optically dense background of dielectric constant ε.

High efficiency of the algorithms over the plane-wave method is achieved due to the employment of appropriate basis functions in the Rayleigh–Ritz method corresponding to relevant eigenfunctions of an auxiliary exactly solvable 2D problem that only slightly differs from the initial one. Such eigenfunctions better approximate the eigenfunctions of the initial problem that results in the faster convergence of the method over the plane-wave approach. The use of the phase method makes possible precise computation of a large number of the basis functions. Fast performance of the code makes it very practical for the optimal design of 2D photonic crystals.

ACKNOWLEDGMENT AND DISCLAIMER

The effort of A. Figotin and Yu. Godin are sponsored by the Air Force Office of Scientific Research, Air Force Materials Command, USAF, under Grant F49620-94-1-0172. The views and conclusions contained herein are those of the authors and should not be interpreted as necessarily representing the official policies or endorsements, either expressed or implied, of the Air Force Office of Scientific Research or the U.S. Government.

REFERENCES

1. N. W. Ashcroft and N. D. Mermin, *Solid State Physics* (Holt, Rinehart, & Winston, New York, 1976).
2. L. C. Botten, M. S. Craig, R. C. McPhedran, J. L. Adams, and J. R. Andrewartha, *Opt. Acta* **28**(8), 413 (1981).
3. *Development and Applications of Materials Exhibiting Photonic Band Gaps*, *J. Opt. Soc. Am. B* **10,** 280 (1993).
4. J. Drake and A. Genack, *Phys. Rev. Lett.* **63,** 259 (1989).
5. E. N. Economou and A. Zdetsis, *Phys. Rev. B* **40,** 1334 (1989).
6. J. M. Elson and P. Tran, *Phys. Rev. B* **54,** 1711 (1996).
7. K. M. Ho, C. T. Chan, and C. M. Soukoulis, *Phys. Rev. Lett.* **65,** 3152 (1990).
8. A. Figotin and P. Kuchment, *SIAM J. Appl. Math.* **56,** 68 (1996).
9. A. Figotin and P. Kuchment, *SIAM J. Appl. Math.* **56,** 1561 (1996).
10. P. Kuchment and I. Ponomaryov, preprint.
11. J. D. Jackson, *Classical Electrodynamics* (Wiley, New York, 1975).
12. S. John, *Phys. Today*, ***May,*** 32 (1991).
13. S. John, The localization of light, in *Photonic Band Gaps and Localization*, edited by C. M. Soukoulis (Plenum, New York, 1993), p. 1. [NATO ASI Series B, Vol. **308**]
14. J. D. Joannopoulos, R. D. Meade, and J. N. Winn, *Photonic Crystals.*

Molding the Flow of Light (Princeton Univ. Press, Princeton, NJ, 1995).
15. K. M. Leung and Y. F. Liu, *Phys. Rev. Lett.* **65,** 2646 (1990).
16. A. A. Maradudin and A. R. McGurn, *J. Opt. Soc. Am. B* **10,** 307 (1993).
17. S. L. McCall, P. M. Platzman, R. Dalichaouch, D. Smith, and S. Schultz, *Phys. Rev. Lett.* **67,** 2017 (1991).
18. R. D. Meade, K. D. Brommer, A. M. Rapper, and J. D. Joannopoulos, *Appl. Phys. Lett.* **61,** 495 (1992).
19. J. B. Pendry and P. M. Bell, Transfer matrix techniques for electromagnetic waves, in *Photonic Band Gap Materials*, edited by C. M. Soukoulis (Kluwer, Dordrecht, 1996), p. 203. [NATO ASI Series E, Vol. **315**]
20. M. Plihal and A. A. Maradudin, *Phys. Rev. B* **44,** 8565 (1991).
21. P. Sheng (Ed.), *Scattering and Localization of Classical Waves* (World Sci., Philadelphia, 1990).
22. M. Sigalas, C. M. Soukoulis, E. N. Economou, C. T. Chan, and K. M. Ho, *Phys. Rev. B* **48,** 14121 (1993).
23. H. S. Sözüer, J. W. Haus, and R. Inguva, *Phys. Rev. B* **45,** 13962 (1992).
24. M. P. Van Albada and A. Lagendijk, *Phys. Rev. Lett.* **55,** 2692 (1985).
25. P. R. Villeneure and M. Piché, *J. Opt. Soc. Am. A* **8,** 1296 (1991).
26. J. R. Wendt, G. A. Vawter, P. L. Gourley, T. M. Brennan, and B. E. Hammons, *J. Vac. Sci. Technol. B* **11**(6), 2637 (1993).
27. E. Yablonovitch and T. J. Gmitter, *Phys. Rev. Lett.* **63,** 1950 (1989).